Solar Energy Materials & Solar Cells 144 (2016) 445–450

Contents lists available at ScienceDirect

Solar Energy Materials & Solar Cells

journal homepage: www.elsevier.com/locate/solmat

The oxidation effect of a Mo back contact on Cu(In,Ga)(Se,S)$_2$ thin-film solar modules

Junggyu Nam [a], Yoonmook Kang [b], Dongseop Kim [a], Dohyun Baek [a], Dongho Lee [a,*], JungYup Yang [a,*]

[a] PV Development Team, Energy Solution Business Division, Samsung SDI, 467, Beonyeong-ro, Seobuk-gu, Cheonan-si, Chungcheongnam-do 331-330, Republic of Korea

[b] Green School, Graduate school of Energy and Environment, 145 Anam-ro, Seongbuk-gu, Seoul 136-713, Republic of Korea

ARTICLE INFO

Article history:
Received 5 April 2015
Received in revised form
1 July 2015
Accepted 24 September 2015
Available online 23 October 2015

Keywords:
Mo back contact
Mo oxidation
CIGSS module
Pattern
Na effect

ABSTRACT

We investigated the surface properties of a Mo back contact for large-area thin-film solar modules with high efficiency and good adhesion between Mo and the absorber layer. It was determined that the appropriate surface properties of Mo would improve the efficiency from 10% to above 15.0 ± 0.21% and narrow the efficiency distribution in large-area modules. The Mo back contact was annealed at various temperatures between room temperature and 230 °C in air to control the amount of sodium diffusing from the soda-lime glass substrate during selenization and sulfurization, and to improve the uniformity of the unit cell. Before the heat treatment, the amount of sodium in the patterned area of the unit cell was more than 10 times of that in the central area of the cell. The patterned region with higher Na content had smaller grains than those in the central area with less Na, resulting in many peel-offs and shunting paths. The difference in sodium content was reduced after heat treatment. The optimized surface oxide of the Mo back contact had a thickness of around 3–5 nm and consisted of the MoO_3 phase. The grain boundary of Mo columnar structure near the surface consisted of the oxide layer.

1. Introduction

The Mo back contact plays important roles in a solar cell, such as the collector of generated carriers and controller of the path of Na diffusion from a soda-lime glass substrate [1–4]. In a Cu(In,Ga)(Se,S)$_2$ (CIGSS) thin-film solar cell prepared by the H_2Se–H_2S reacting gas, the metal back contact should be resistant against the Se reaction in a hydrogen atmosphere during high-temperature selenization. A Mo back contact is commonly used because Mo has an appropriately high work function for an ohmic contact and can resist etching in a high-temperature process sequence. The Mo compounds produced in the process, such as $MoSe_2$, MoS_2, or Mo(Se,S)$_2$, have the appropriate lubricating property to assist sliding of the scribe needle [4–7]. $MoSe_2$ offers the advantage of being able to reduce the resistance between the CIGSS layer and Mo back contact with an ohmic contact [8–10]. However, $MoSe_2$ and MoS_2 are semiconductors with direct bandgaps, and if values of their layer thickness increase beyond hundreds of nanometers, the series resistance will be increased, especially for MoS_2 [11]. It has been reported that the properties and qualities of the back contact may depend on the surface conditions of the Mo layer, such as the oxidation state of the surface [11,12].

In this report, we focus on the advantages of the thin Mo oxide layer on the surface of the Mo contact for fabricating monolithic thin-film CIGSS solar modules. It is well known that many peel-offs can be found at the CIGSS–Mo interface near P1 patterns and in the middle of the cell if there is an oversupply of Na to the CIGSS absorber thin film. We will show the peel-offs have several origins in a large-area module, and we will discuss the process used to reduce such peel-offs. We will also present an analysis of thin-film properties obtained by secondary ion mass spectroscopy (SIMS), X-ray photoelectron spectroscopy (XPS), transmission electron microscopy (TEM), scanning electron microscopy (SEM), and shunt infrared (IR) imaging.

2. Experimental details

Thin films of CIGSS were prepared by sputtering and sequential selenization in a H_2Se (99.99%, 4N) atmosphere and sulfurization

Abbreviations: BZO, boron-doped zinc oxide; CBD, chemical bath deposition; CIGSS, copper–indium–gallium–sulfur selenide, Cu(In,Ga)(Se,S)$_2$; FF, fill factor; IR imaging, infrared imaging; LPCVD, low-pressure chemical vapor deposition; SEM, scanning electron microscopy; SIMS, secondary ion mass spectroscopy; TCO, transparent conductive oxide; TEM, transmission electron microscopy; XPS, X-ray photoelectron spectroscopy

* Corresponding authors.
E-mail addresses: dhlee0333@gmail.com (D. Lee), jungyupyang@gmail.com (J. Yang).

http://dx.doi.org/10.1016/j.solmat.2015.09.035
0927-0248/

in a H_2S (99.99%, 4N) atmosphere with N_2 in the furnace. A Cu–Ga–In metal alloy thin film was first deposited by DC magnetron sputtering with a rotary target before it was placed in a reaction furnace for sequential processing. The thickness of the thin film was controlled to adjust for the final CIGSS layer thickness after the processes. The back contact Mo layer was deposited by DC magnetron sputtering before the precursor thin film was deposited on the soda-lime glass substrate, which had a high strain point at temperatures above 600 °C when compared with normal soda-lime glass. For a monolithically integrated solar module, we scribed the Mo layer with a high-power laser for the first pattern (P1). The P1 width and adjacent P1 scribing were optimized based on the desired current density and transparent conductive oxide (TCO) thickness and quality. The oxidation of the Mo back contact was performed in air in a convection oven at several temperatures between room temperature and 230 °C for 20 min after P1 laser patterning. For the analysis of properties of the oxidized surface film, we deposited a capping layer on the Mo thin film to exclude the effect of the atmosphere before and after oxidation in the furnace. The buffer layer for reducing the number of shunting paths and increasing the interface quality was grown on the absorber layer via chemical bath deposition (CBD). The ZnS(O,OH)-based buffer layer was deposited using chemical sources such as $ZnSO_4$, NH_4OH, and thiourea dissolved in deionized (DI) water for 15 min. After the CBD process, mechanical scribing for the second pattern (P2) was performed to establish series connection between the unit cells isolated by P1. The gap between P1 and P2 was minimized to reduce the dead area in the total module area. Boron-doped ZnO (BZO) was deposited on the CBD buffer layer as a TCO window layer via low-pressure chemical vapor deposition (LPCVD). The final step of cutting the TCO layer to isolate the unit cell for modularization was carried out by mechanical scribing of the third pattern (P3).

The morphology of the thin film near the patterns was analyzed by SEM, and the electric properties were examined by reverse-biased shunt IR imaging. The depth profile of the thin film before and after oxidation was compared by SIMS. The morphologies of non-oxidized and oxidized Mo layers were also analyzed by XPS and TEM by measuring the layer thickness and characterizing the phase of the thin oxide layer. The efficiency of the prepared large-area modules was checked under calibrated AM 1.5G illumination in our pilot line.

3. Results and discussion

We performed precise electrical and physical analyses to investigate the direct contacts within this solar device. A shunt IR image of the module and the optical and shunt IR images of a cell in the CIGSS module are shown in Fig. 1(a)–(c), respectively. Many red spots are visible in Fig. 1(a), which depend on the direct contact between the Mo back contact and TCO layer when the CIGSS layer peeled off from the Mo back contact during processing. The shunt IR image shows that the heat originated from the ohmic contact in reverse biasing on the p–n junction of the solar device. This kind of ohmic contact creates shunting paths in real-life application and should be removed. The points P, C, and E in Fig. 1(b) and (c) indicate the range of patterns, the center of a cell, and the intermediate range between P and C, respectively. The optical image in Fig. 1(b) shows a different color at each site, while the electron microscope reverse-biased shunt IR image in Fig. 1(c) shows red spots at the center of each cell when measured at high resolution. During the preparation of the monolithic thin-film CIGSS solar module, when the heat treatment was performed to synthesize the absorber ($CIGSe_2$ or CIGSS) layer at high temperature, alkali elements such as Na and K were transported from the glass substrate into the CIGSS absorber layer through the Mo back contact [14–16]. In general, a larger quantity of the elements should be detected near the patterns because they were removed by the laser source for isolation from the Mo back contact. Other researchers have reported the effect of sodium from the point of view of grain growth and the crystallization [17–20], as well as the stability and passivation of the absorber layer [21–25]. We, on the other hand, focus on harmful effects in this report, such as the presence of excess Na as the cause of the peel-offs between the Mo back contact and absorber.

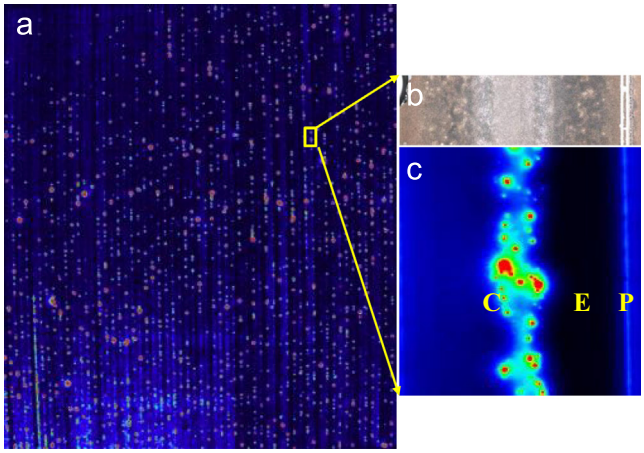

Fig. 1. Images of shunt IR (a) in CIGS module at low resolution and (b) in a unit cell of CIGS module at high resolution. (b) Optical image at the same position where (c) was obtained. The red spots show the ohmic contact at the unit cell. (For interpretation of the references to color in this figure legend, the reader is referred to the web version of this article.)

As mentioned earlier, to elucidate the basic reason for the difference in morphology of the three regions, we performed SEM analysis at points, C, E, and P. Fig. 2 describes cross-sectional SEM images of the film at these points. The grain size at point C was larger than those at points E and P, which were similar to each other. While points E and P had many voids between Mo and the CIGSS layer, none of them were observed at point C. Fig. 2(c) shows the regular voids generated by sputtering and sequential processing due to the expansion of the metal precursor and the reaction rate. The image of E in Fig. 2(b) depicts the larger voids with an irregular size. Fig. 3 shows the top-view of the same area measured by SEM at high resolution. In Fig. 3(a), the P region had a flat and smooth surface and the E region had irregularities on the surface. Many cavities were created by the CIGSS layer peeling off from the Mo back contact in the C region, as shown Fig. 3(b). It could be assumed that the difference in brightness in the three regions in Fig. 1(b) stemmed from the difference in reflection at the CIGSS surface as a result of the surface roughness. Based on these results, it appears that the ohmic contacts were created when the CIGSS layer peeled off from the Mo back contact at many points during selenization and sulfurization, and then TCO was deposited on the resulting cavities. To determine the reason for the peel-offs from the Mo back contact, we made the following assumptions: the difference in morphology was caused by the amount of transferred materials from the glass substrate; the peel-off at point C and the shape of embossing at point E originated from the difference in stress in different regions of the thin film owing to the different morphologies, such as grain size and void shape, in the regions. We first analyzed the Mo thin film to evaluate the validity of our assumptions at each point. Fig. 4 shows that a larger amount of surface oxygen resided at point P than point C. Since oxygen can assist the diffusion of alkali metals [1,26–29], the constituent elements of the absorber could have been changed after selenization. Although the above assumption has not been confirmed and more investigation is needed, we can make the following deductions: (1) The laser source for P1

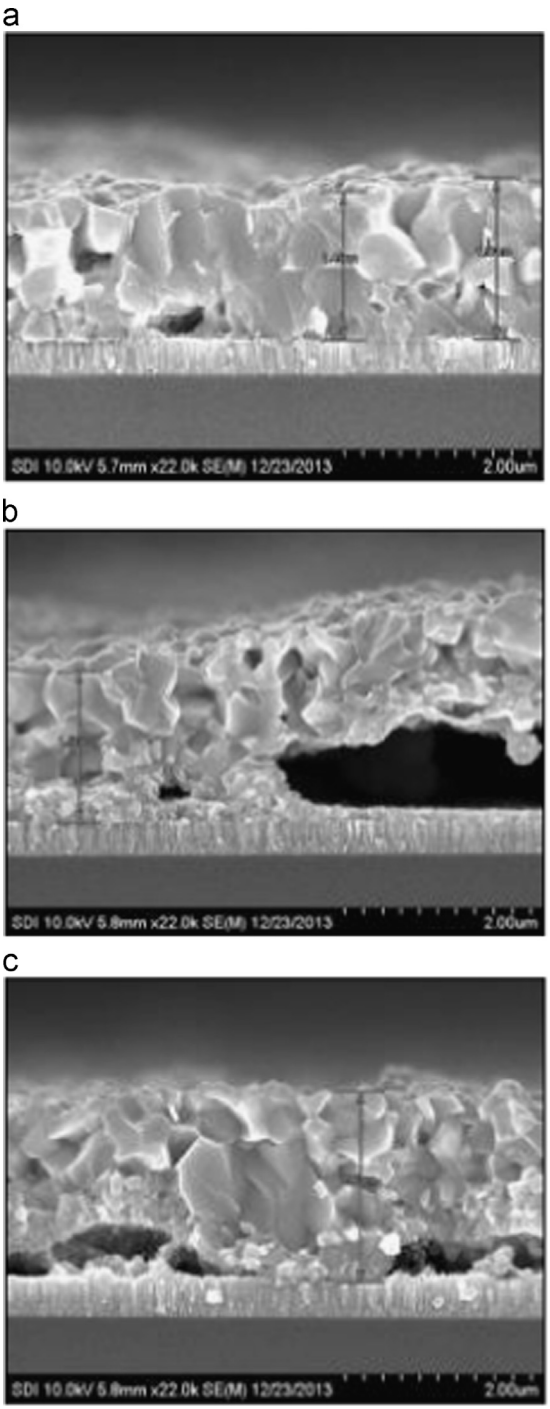

Fig. 2. SEM images showing the morphology of in the regions around points (a) C, (b) E, and (c) P in Fig. 1. The grain size, void shape, and void size at the interface between the CIGSS layer and the Mo back contact were quite different in each region.

patterning must have affected the Mo back contact. In Fig. 2, the surface morphologies at points C, P, and E remained unchanged up to a similar distance on both sides from the P1 pattern. (2) The different amount of residual water at each point after P1 cleaning might have affected the surface state of the Mo back contact. After P1 patterning, the patterned area showed a regular unevenness and the center area exhibited a flat fresh Mo surface. Therefore, the amount of residual water after P1 cleaning by deionized water should be different at each point. Therefore, we can conclude that the Mo back contact had a different surface state at each point, P

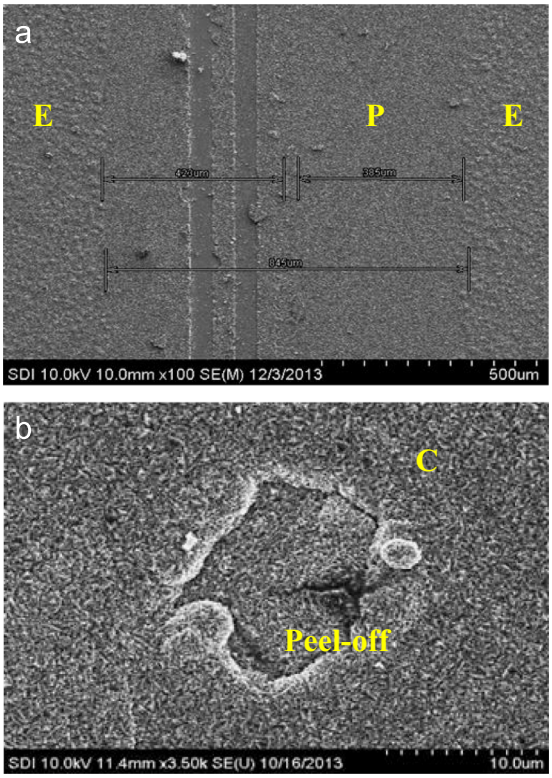

Fig. 3. Top-view SEM images of the three regions around points C, E, and P. Points E and P had different appearances, with E rougher than P. The cavity at C was caused by the peel-off of the CIGSS layer.

and C, prior to the precursor deposition and after sequential selenization and sulfurization. In the case of a monolithic thin-film module, the non-uniformity issues presented above are inevitable if the patterns are formed by laser irradiation; if the power of the laser source is changed, isolation issues could occur and many burrs could be formed excessively. Such as two kinds of changes should decrease the open circuit voltage and fill factor due to the connection of two unit cells and due to making a lot of shunting paths respectively.

As mentioned earlier, the surface oxygen content was different at each point and oxygen affected the diffusion of elements such as Na and K from the glass substrate when heat treatment was performed at high temperature for a long time. In order to obtain a uniform surface state of the Mo thin film, we investigated the state of its oxidation. Fig. 5 shows the oxidation properties of the Mo back contact at several temperatures of heat treatment for removing the non-uniformity issues. The Mo thin film was placed into the furnace in an air atmosphere and its oxygen content at the surface increased with increasing heating temperature. The phase of the resulting oxide consisted of MoO_2 and MoO_3. The concentration of MoO_3 increased and the concentration of MoO_2 decreased with increasing heating temperature. Since MoO_2 is a semiconductor and MoO_3 is an insulator, they have different material properties. If MoO_2 and MoO_3 had remained after selenization and sulfurization, different device properties would have emerged. Regardless, Mo oxide properties were not an issue in our study since the surface oxide was replaced by Se and S during selenization and sulfurization at high temperature. In fact, the surface oxide would have retarded the growth reaction of $Mo(Se,S)_2$ since Se and S were supposed to substitute for oxygen that had bonded with Mo. Moreover, the amount of surface oxide played a role in the change in thickness of $Mo(Se,S)_2$. A Mo chalcogenide compound is a semiconductor and it helped the formation of ohmic contact between the CIGSS layer and Mo back contact;

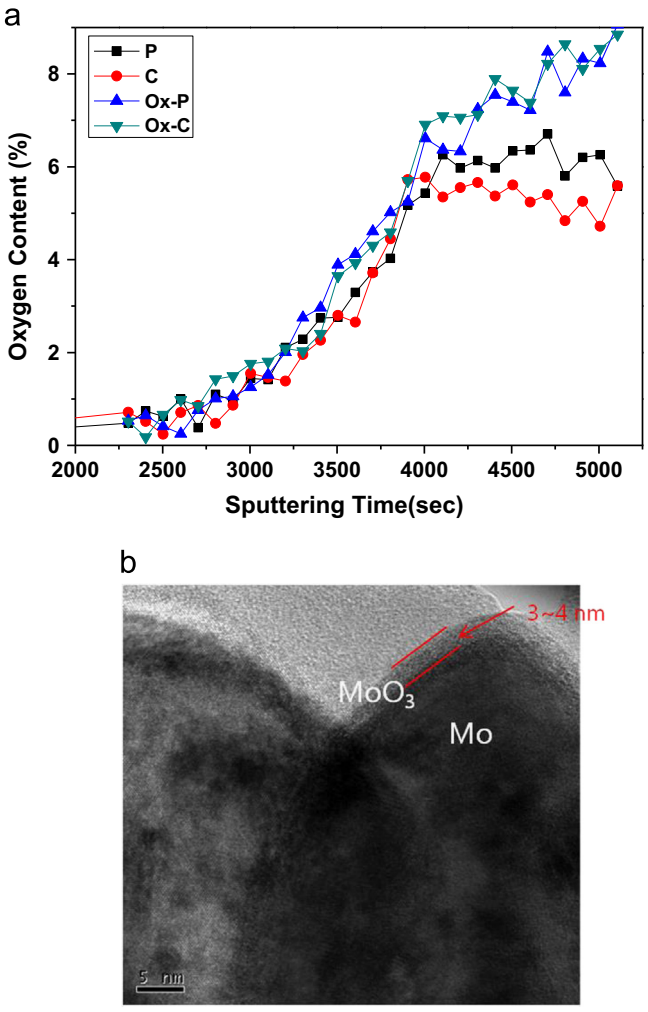

Fig. 4. (a) XPS depth profile of oxygen at the bare Mo back contact. The lines labeled P and C show the profiles before oxidation and the lines labeled Ox-P and Ox-C show the profiles after oxidation. (b) Image of the optimized oxide layer on the Mo back contact.

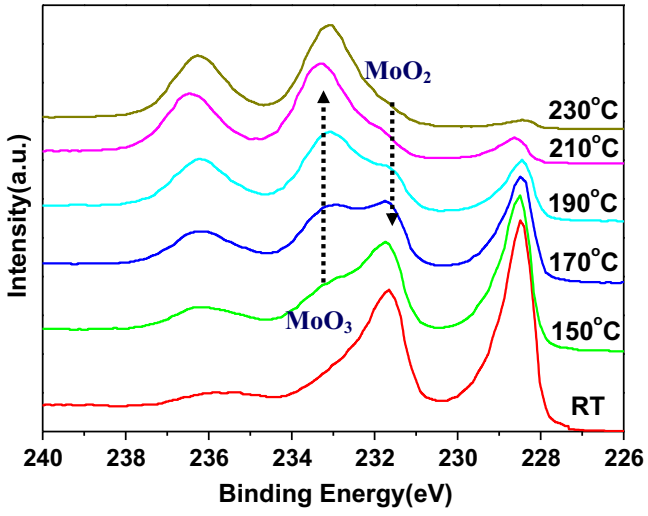

Fig. 5. XPS results of oxidization of the Mo back contact from room temperature to 230 °C.

however, if the thickness had grown beyond a certain value, it would become a barrier to the transfer of hole carriers against the Mo back contact. Table 1 lists the amount of MoO_2, MoO_3, and MoO_2+MoO_3 calculated from the area under the curve at each temperature in Fig. 5. The best performance was obtained at near 80% Mo oxide from XPS analysis when the device was evaluated after heat treatment at several temperatures. Fig. 4(b) shows the TEM morphology of Mo thin film after heat treatment under optimized conditions. The oxide layer was formed at a depth of 5 nm from the surface and grain boundary near the surface. As mentioned earlier, that oxygen should affect the diffusion of alkali elements from the glass substrate. In addition, oxygen that diffused into the CIGSS layer during selenization should have played a role in catalysis with Na to the reaction of selenization.

Table 1
Ratio of Mo, MoO_2, and MoO_3 content after heat treatment at temperatures between room temperature and 230 °C.

Temperature		Conc. (%)	MoO_2+MoO_3
No bake	Mo metal	55.8	44.20
	MoO_2	23.1	
	MoO_3	21.1	
150 °C Bake	Mo metal	40.5	59.50
	MoO_2	23.3	
	MoO_3	36.2	
170 °C Bake	Mo metal	31.3	68.70
	MoO_2	16.7	
	MoO_3	52	
190 °C Bake	Mo metal	20.5	79.50
	MoO_2	9.9	
	MoO_3	69.6	
210 °C Bake	Mo metal	11.4	88.60
	MoO_2	2.2	
	MoO_3	86.4	
230 °C Bake	Mo metal	5.6	94.40
	MoO_2	0	
	MoO_3	94.4	

Fig. 4 shows the results of XPS analysis of the Mo thin film after heat treatment under optimized conditions based on the above evaluations. The surface oxygen content was higher before the heat treatment in air, and both points P and C had similar oxygen content throughout the same depth within the Mo thin film. As shown in Fig. 6, when the Mo back contact was prepared by the optimized process, the gap in Na content at each point was reduced drastically since there were smaller grains, such as those shown at points E and P in Fig. 2, at the grain boundary. Before heat treatment, there was not much difference between the Na content at points P and E; however, the Na content was especially low at point E after oxidation. We already confirmed that the grain size was very large at point E. In general, Na usually resides at the grain boundary more often than within the grain [29,30]. In the case of Ga, the depth profile was correlated with the grain size distribution. Although it is generally difficult for different phases to co-exist in one grain, CIGSS has a band grading in one grain based on different compositional ratios, and the difference in band gap calculated from the compositional ratio is within 0.1 eV [13]. In this process, the calculated bandgap grading of P and E was above 0.5 eV from bottom to top, and the band grading at C point was very small since Ga was out-diffusing very quickly, as shown Fig. 6(b). We assume that those kinds of state were related to Na diffusion from the glass substrate, resulting in the non-uniformity. When the heat-treated Mo thin film was used, the Na content at point C was smaller than those at points P and E; however, the gap among the three points was drastically reduced since the uniformity of Mo thin film was improved. We can suggest that the surface oxidation of Mo thin film in monolithic modules with patterns improves the uniformity of the unit cell and reduces cell failure from shunting paths, for example. The reduction in the number of shunting path should lead to an increase in the open

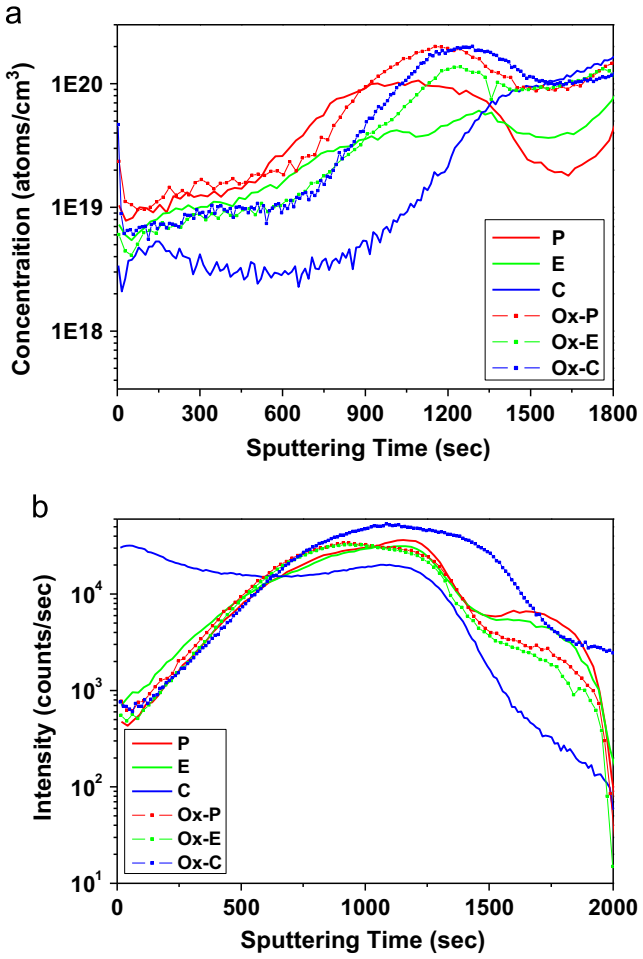

Fig. 6. SIMS depth profile of Na (a) and Ga (b) in the CIGSS layer before and after oxidation.

circuit voltage and the fill factor because of the increase in shunt resistance and the decrease in ideality factor (*n*-factor).

Fig. 7 shows the shunt IR image of a CIGSS thin-film solar module prepared with the optimized Mo back contact. Compared to the image in Fig. 1(a) of the Mo back contact before optimization, the number of red spots was drastically reduced. Fig. 8 shows the efficiency parameters of a large-area (902×1602 mm^2) module. After the new optimized Mo back contact was used in the preparation process, the efficiency was drastically increased because the open-circuit voltage and fill factor depended on the shunting paths. Compared with the short-circuit current before oxidation, the short-circuit current was not directly related to the efficiency after oxidation. This experiment was conducted using just one slot. The average and the standard deviation of efficiency were 15.0% and 0.21%, the latter of which is very narrow for each parameter.

4. Conclusions

In the fabricating process of a monolithic thin-film module, non-uniformity within the unit cell resulting from laser patterning and P1 cleaning occurs and the shunt resistance decreases because of the abundance of shunting paths. To avoid this kind of problem and to obtain a more uniform surface state of the Mo back contact, the Mo back contact was oxidized in air at several temperatures after P1 cleaning. The surface thin oxide contributed to the transfer of elemental constituents from the glass substrate. The

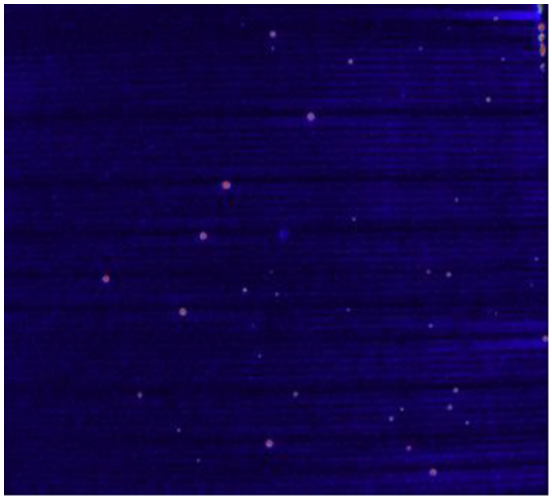

Fig. 7. Shunting IR Image of CIGSS module after oxidation. (For interpretation of the references to color in this figure, the reader is referred to the web version of this article.)

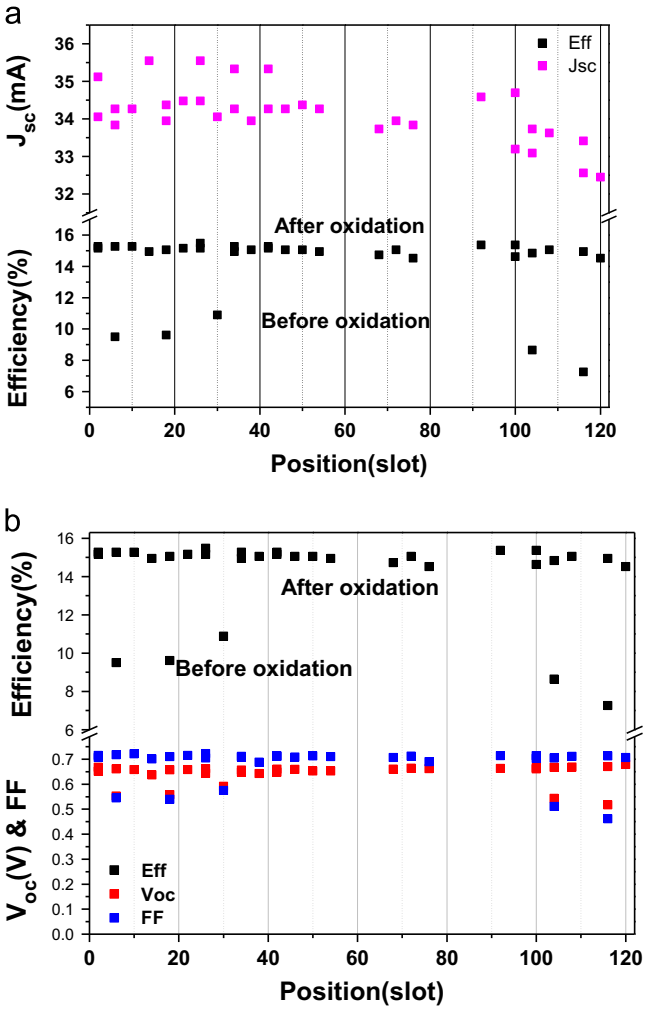

Fig. 8. Comparison of efficiency and efficiency parameters of a large-area CIGSS module. The change in efficiency was dependent on FF and V_{oc}; however, J_{sc} had low impact on the module efficiency.

CIGSS thin-film solar module exhibited the best properties when the ratio of Mo metal to Mo oxide was close to 0.8. The controlled CIGSS layer utilized by the oxidized Mo thin film had more

uniform grain size and depth profile for each element. The module efficiency had a narrow distribution, $15.0 \pm 0.21\%$, for an area of 902×1602 mm^2.

Acknowledgments

The authors thank their colleagues at the PV Development Team and Core Technology Laboratory of Samsung SDI. This work was supported by the Korea Institute of Energy Technology Evaluation and Planning (KETEP) (Grant no. 20119010100010) in 2011 and by the National Research Foundation of Korea Grant funded by the Korean Government (MSIP) (2015, University-Institute cooperation program).

References

[1] J.-H. Yoon, T.-Y. Seong, J.-H. Jeong, Effect of a Mo back contact on Na diffusion in CIGS thin film solar cells, Prog. Photovolt. 21 (2013) 58–63.
[2] J.H. Scofield, Sodium diffusion, selenization, and microstructural effects associated with various molybdenum back contact layers for CIS-based solar cells, in: Conference Record of the 24th IEEE Photovoltaic Specialists Conference – 1994 IEEE First World Conference on Photovoltaic Energy Conversion, IEEE, New York, 1995, pp. 164–167.
[3] A. Rockett, K. Granath, S. Asher, M.M. Al Jassim, F. Hasoon, R. Matson, B. Basol, V. Kapur, J.S. Britt, T. Gillespie, C. Marshall, Na incorporation in Mo and $CuInSe_2$ from production processes, Sol. Energy Mater. Sol. Cells 59 (1999) 255–264.
[4] H.A. Al-Thani, F.S. Hasoon, M. Young, S. Asher, J.L. Alleman, M.M. Al-Jassim, D.L. Williamson, The effect of Mo back contact on Na out-diffusion and device performance of Mo/Cu(In,Ga)Se_2/CdS/ZnO solar cells, in: Conference Record of the 29th IEEE Photovoltaic Specialists Conference, IEEE, New York, 2002, pp. 720–723.
[5] R. Krishnan, E.A. Payzant, R. Kacnyzki, U. Schoop, J. Britt, R. Noufi, T.J. Anderson, Reaction kinetics and pathways of $MoSe_2$, in: Proceedings of the 35th IEEE Photovoltaic Specialists Conference, IEEE, New York, 2010, pp. 1006–1008.
[6] K. Kushiya, M. Tachiyuki, Y. Nagoya, A. Fujimaki, B. Sang, D. Okumura, M. Satoh., O. Yamase, Progress in large-area Cu(InGa)Se_2-based thin-film modules with a $Zn(O,S,OH)_x$ buffer layer, Sol. Energy Mater. Sol. Cells 67 (2001) 11–20.
[7] D.E. Tarrant, R.R. Gay, Process R&D for CIS-based Thin-film PV, NREL, United States (2006), p. 02–05 , Final Technical Report.
[8] N. Kohara, S. Nishiwaki, Y. Hashimoto, T. Negami, T. Wada, Electrical properties of the Cu(In,Ga)Se_2/$MoSe_2$/Mo structure, Sol. Energy Mater. Sol. Cells 67 (2001) 209–215.
[9] T. Wada, N. Kohara, S. Nishiwaki, T. Negami, Characterization of the Cu(In,Ga)Se_2/Mo interface in CIGS solar cells, Thin Solid Films 387 (2001) 118–122.
[10] A. Mallousky, J. Bernede, Characterization of $MoSe_2$ thin films, Thin Solid Films 158 (1988) 285–298.
[11] D.C. Fisher, I.L. Repins, J. Schaefer, M.E. Beck, W.K. Batchelor, M. Young, S. Asher, The effect of Mo morphology on the performance of Cu(In,Ga)Se_2 thin films, in: Proceedings of the 31st IEEE Photovoltaic Specialists Conference, IEEE, New York, 2005.
[12] P. Salome, V. Fjallstrom, A. Hultqvist, P. Szanianwski, U. Zimmermann, M. Edoff, The effect of Mo back contact ageing on Cu(In,Ga)Se_2 thin-film solar cells, Prog. Photovolt. 22 (2014) 83–89.
[13] I. Repins, S. Glynn, J. Duenow, T.J. Coutts, W. Metzger, M.A. Contreras, Required Materials Properties for High-efficiency CIGS Modules, Conference paper NREL/CP-520-46235, July 2009.
[14] M. Ruckh, D. Schmid, M. Kaiser, R. Schaffler, T. Walter, H.W. Schock, Influence of substrates on the electrical properties of Cu(In,Ga)Se_2 thin films, in: Conference Record of the 24th IEEE Photovoltaic Specialists Conference – 1994 IEEE First World Conference on Photovoltaic Energy Conversion 1994, IEEE, New York, 1995, pp. 156–159.
[15] R.J. Matson, J.E. Granata, S.E. Asher, M.R. Young, Effects of substrate and Na concentration on device properties, junction formation, and film microstructure in CIS PV devices, in: NCPV Photovoltaics Program Review: Proceedings of the 15th Conference, vol. 462, 1998, pp. 542–549.
[16] A. Rockett, J.S. Britt, T. Gillespie, C. Marshall, M.M. Al-Jassim, F. Hasoon, R. Matson, B. Basol, Na in selenized Cu(In,Ga)Se_2 on Na-containing and Na-free glasses: distribution, grain structure, and device performances, Thin Solid Films 372 (2000) 212–217.
[17] D. Braunger, D. Hariskos, G. Bilger, U. Rau, H.W. Schock, Influence of sodium on the growth of polycrystalline Cu(In,Ga)Se_2 thin films, Thin Solid Films 361–362 (2000) 161–166.
[18] W.N. Shafarman, J. Zhu, Morphology and deposition temperature on CIGS solar cells, Mater. Res. Soc. Symp. Proc. 668 (2001) H2.3.1–H2.3.6.
[19] R. Kimura, T. Mouri, T. Nakada, S. Niki, Y. Lacroix, T. Matsuzawa, K. Takahashi, A. Kunioka, Photoluminescence properties of sodium incorporated in $CuInSe_2$ thin films, Jpn. J. Appl. Phys. 38 (1999) L289–L291.
[20] M.A. Contreras, B. Egaas, P. Dippo, J. Webb, J. Granata, K. Ramanathan, S. Asher, A. Swartzlander, R. Noufi, On the role of Na and modifications to CIGS absorber materials using thin MF (M=Na, K, Cs) precursor layers, in: Conference Record of the 26th IEEE Photovoltaic Specialists Conference, IEEE, New York, 1997, pp. 359–362.
[21] T. Nakada, H. Ohbo, M. Fukuda, A. Kunioka, Improved compositional flexibility of CIGS based thin film solar cells by sodium control technique, Sol. Energy Mater. Sol. Cells 49 (1997) 261–267.
[22] K. Granath, M. Bodegard, L. Stolt, The effect of NaF on Cu(In,Ga)Se_2 thin film solar cells, Sol. Energy Mater. Sol. Cells 60 (2000) 279–293.
[23] J.E. Granata, J.R. Sites, S. Asher, R. Matson, Quantitative incorporation of sodium in $CuInSe_2$ and Cu(In,Ga)Se_2 photovoltaic devices, in: Conference Record of the Twenty Sixth IEEE Photovoltaic Specialists Conference, IEEE, New York, 1997, pp. 387–390.
[24] J.E. Granata, J.R. Sites, Impact of sodium in the bulk and in grain boundaries of CIS, in: Proceedings of the 2nd World Conference on Photovoltaic Solar Energy Conversion, 1998, pp. 604–607.
[25] V. Probst, F. Karg, J. Rimmasch, W. Riedl, W. Stetter, H. Harms, O. Eibl, Advanced stacked elemental layer process for CIGS thin-film photovoltaic devices, Mater. Res. Soc. Symp. Proc. 426 (1996) 165–176.
[26] M. Bodegard, K. Granath, L. Stolt, A. Rockett, The behavior of Na implant into Mo thin films during annealing, Sol. Energy Mater. Sol. Cells 58 (1999) 199–208.
[27] M.B. Zellner, R.W. Birkmire, E. Eser, W.N. Sharfarman, J.G. Chen, Determination of activation barriers for the diffusion of sodium through CIGS thin-film solar cells, Prog. Photovolt. 11 (2003) 543–548.
[28] R.V. Forest, E. Eser, B.E. McCandless, R.W. Birkmire, J.G. Chen, Understanding the role of oxygen in the segregation of sodium at the surface of molybdenum coated soda-lime glass, AIChE J. 60 (2014) 2365–2372.
[29] E. Cadel, N. Barreau, J. Kessler, P. Pareige, Atom probe study of sodium distribution in polycrystalline Cu(In,Ga)Se_2 thin film, Acta Mater. 58 (2010) 2634–2637.
[30] D.W. Niles, M. Al-Jassim, K. Ramanathan, Direct observation of Na and O impurities at grain surfaces of $CuInSe_2$ thin films, J. Vaccum Sci. Technol. A 17 (1999) 291–296.